ACS SyntheticBiology

pubs.acs.org/synthbio

Research Article

Implementation of a Novel Optogenetic Tool in Mammalian Cells Based on a Split T7 RNA Polymerase

Sara Dionisi, Karol Piera, Armin Baumschlager, and Mustafa Khammash*

Cite This: *ACS Synth. Biol.* 2022, 11, 2650−2661

Read Online

ACCESS | Metrics & More | Article Recommendations | Supporting Information

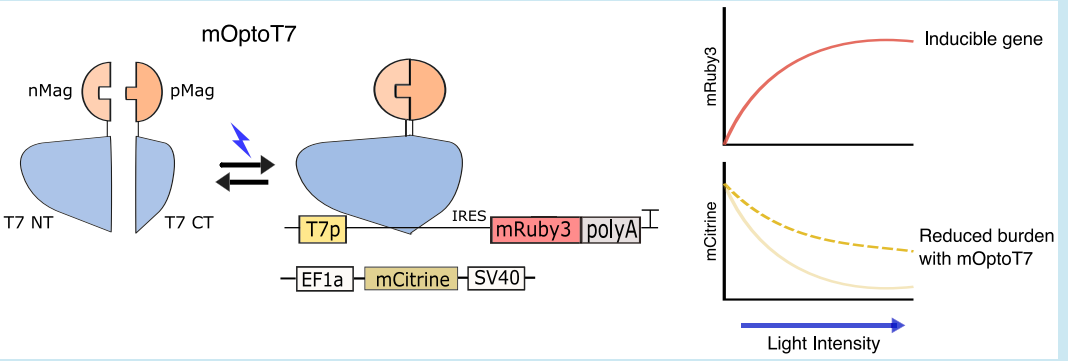

ABSTRACT: Optogenetic tools are widely used to control gene expression dynamics both in prokaryotic and eukaryotic cells. These tools are used in a variety of biological applications from stem cell differentiation to metabolic engineering. Despite some tools already available in bacteria, no light-inducible system currently exists to control gene expression independently from mammalian transcriptional and/or translational machineries thus working orthogonally to endogenous regulatory mechanisms. Such a tool would be particularly important in synthetic biology, where orthogonality is advantageous to achieve robust activation of synthetic networks. Here we implement, characterize, and optimize a new optogenetic tool in mammalian cells based on a previously published system in bacteria called Opto-T7RNAPs. The tool is orthogonal to the cellular machinery for transcription and consists of a split T7 RNA polymerase coupled with the blue light-inducible magnets system (mammalian OptoT7−mOptoT7). In our study we exploited the T7 polymerase's viral origins to tune our system's expression level, reaching up to an almost 20-fold change activation over the dark control. mOptoT7 is used here to generate mRNA for protein expression, shRNA for protein inhibition, and Pepper aptamer for RNA visualization. Moreover, we show that mOptoT7 can mitigate the gene expression burden when compared to another optogenetic construct. These properties make mOptoT7 a powerful new tool to use when orthogonality and viral RNA species (that lack endogenous RNA modifications) are desired.

KEYWORDS: *optogenetics, synthetic biology, gene expression burden, T7 polymerase, light control, dynamic regulation*

INTRODUCTION

The ability to precisely control gene expression in time and space is essential to answer many open questions in biology ranging from development to metabolic processes. Traditional studies that investigate gene expression and function mostly rely on overexpression, knockdowns, or knockouts of the gene of interest.[1−3] This, however, is done at the expense of gaining information on the expression dynamics. In recent years, the field of synthetic biology has helped to address some of these challenges with the use of small molecule regulators, offering powerful tools to control gene expression.[4] For example, systems based on gas or food additives have been used to activate gene expression in the context of genetic circuits.[5−7] However, these approaches are limited by slow dynamics, a lack of spatial control, and burden on the cellular resources. In synthetic biology, resource allocation is one of the main problems associated with engineered genetic circuits. These gene-based networks can create substantial burden on the cellular machineries challenging their use for therapy or downstream applications.[8−10]

Light-inducible ("optogenetic") systems offer major advantages compared to chemical-based approaches.[11−13] These tools allow for tight dynamics, spatial and temporal control, and can regulate gene expression either by activating/repressing genes, or by controlling protein functions. To

Received: February 7, 2022
Published: August 3, 2022

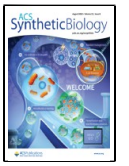

ACS Publications

© 2022 The Authors. Published by American Chemical Society

https://doi.org/10.1021/acssynbio.2c00067
ACS Synth. Biol. 2022, 11, 2650−2661

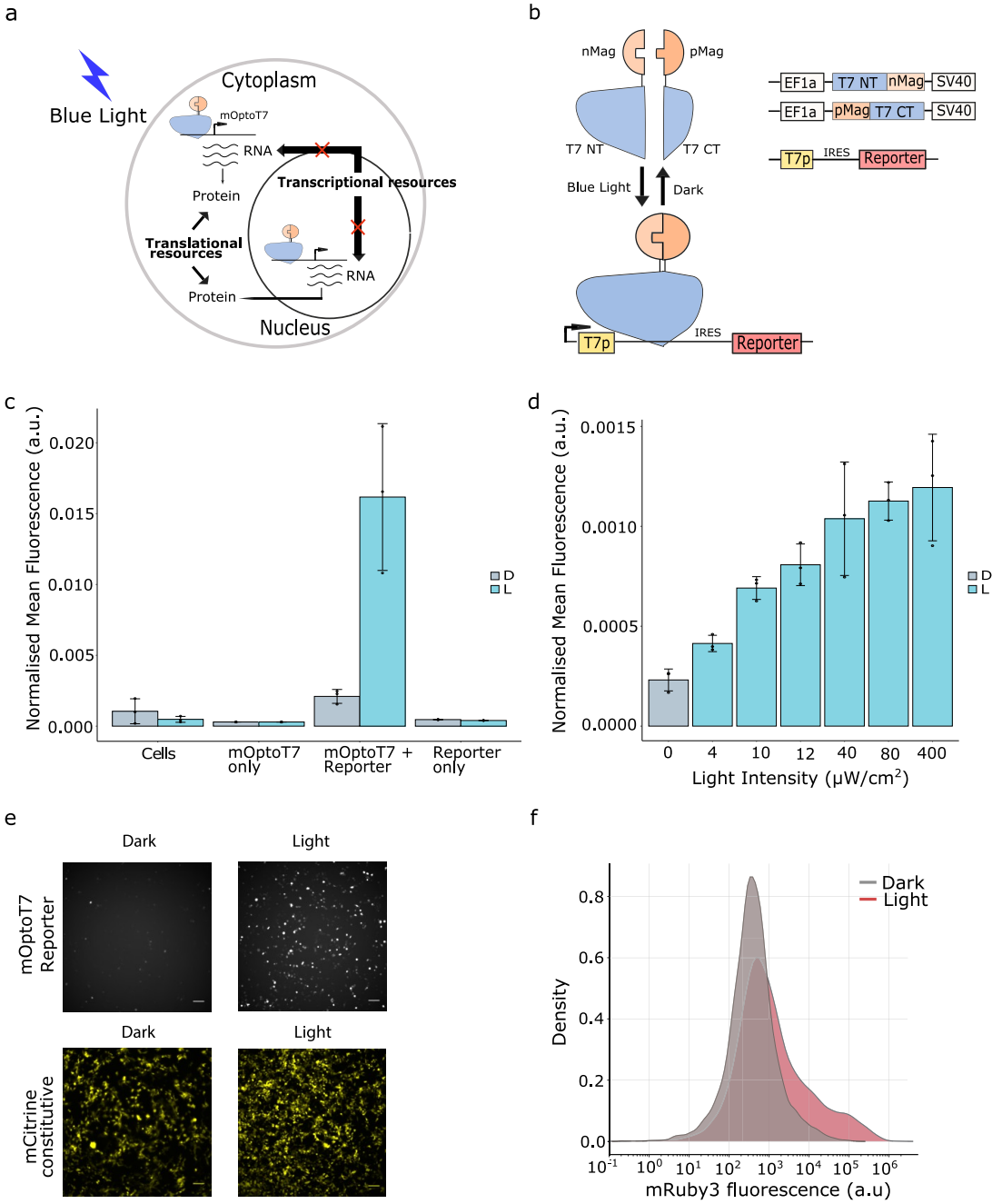

Figure 1. Implementation of mOpto-T7 in HEK293T cells. (a) Overview of mOptoT7 function in mammalian cells. When expressed in HEK293T cells, mOptoT7 can transcribe RNA both in the cytoplasm and in the nucleus. Once it is produced in the cell, mOptoT7 carries out its function independently from the cellular polymerase and transcription factors, making it orthogonal to the cellular machinery for transcription of the reporter gene. (b) Experimental design. mOpto-T7 is transfected in HEK293T cells together with mRuby3 reporter under the control of the T7 promoter. IRES2 sequence is used to allow for translation initiation. (c) Flow cytometry data of mOpto-T7expression after 24 h of constant illumination in saturating conditions. Background fluorescence from only cells and only reporter expression is included. D = dark, L = light. (d) Dose response curve of mOpto-T7 with increasing light illumination. D = dark, L = light. Measurements were taken at the flow cytometer after 24 h of constant illumination. (e) Microscopy images of mRuby3 reporter activation from panel c. mCitrine is used as constitutive color as a measure of transfection efficiency. Scale bar = 100 μm. (f) Kernel density estimation plot showing mRuby3 expression in the dark vs saturating light after 24 h of constant blue light illumination. Flow cytometry data are normalized to the constitutively expressed mCitrine. Saturating light = 400 μW/cm^2.

date, many optogenetic tools are available for both bacterial and mammalian cells.[14,15] However, no optogenetic system can currently be used to produce proteins that are decoupled from the cellular transcriptional and/or translational machineries (hereafter referred to as "orthogonal"); such a tool could be useful for synthetic biology applications where the performance of gene networks is influenced by the interaction with the host regulatory processes.

An optogenetic system that functions orthogonally to the cellular machinery should ideally be independent from all cellular resources. Complete orthogonality is hard if not impossible to achieve; however, in bacteria, this was partly addressed with the use of the T7 RNA polymerase that allows

https://doi.org/10.1021/acssynbio.2c00067
ACS Synth. Biol. 2022, 11, 2650−2661

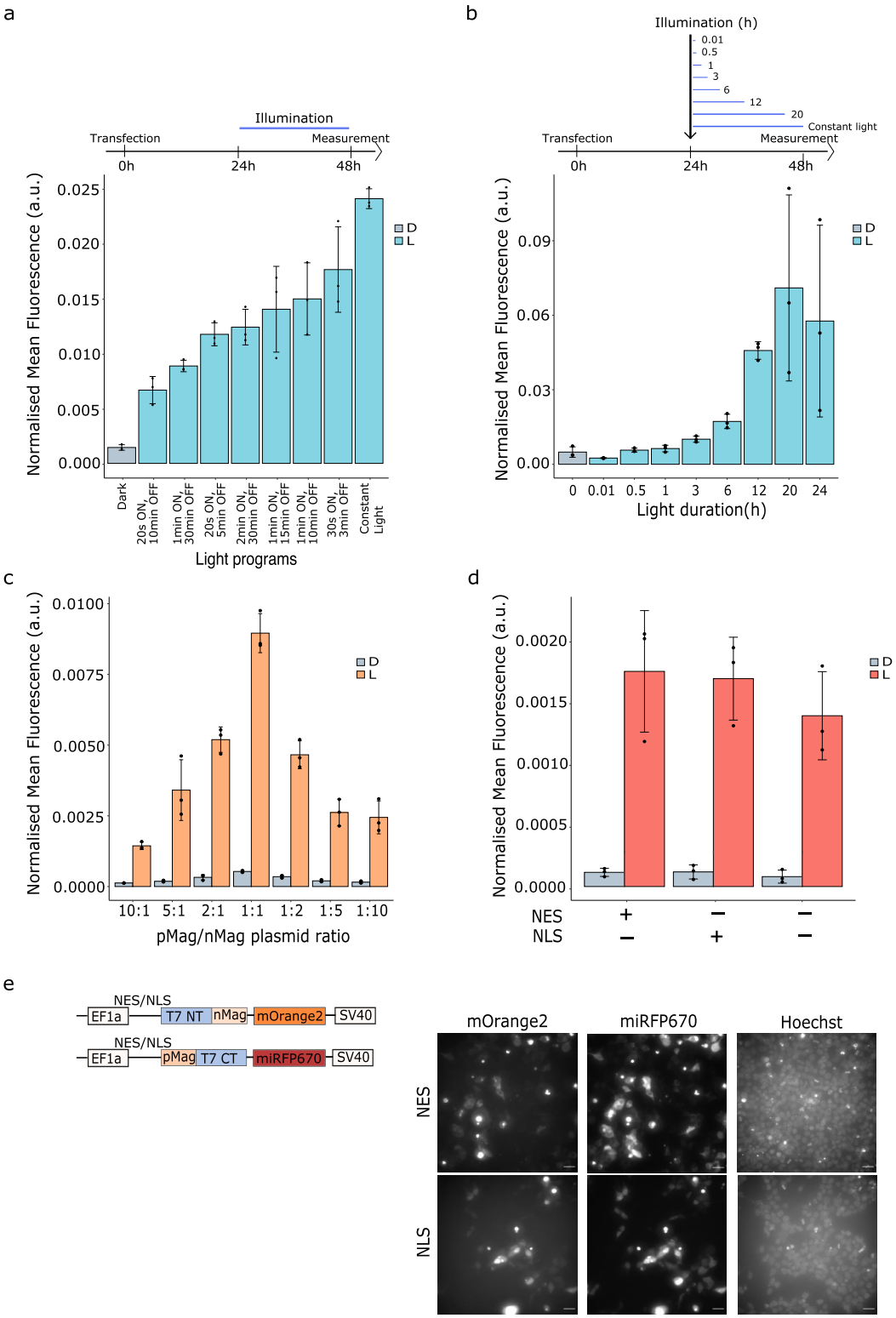

Figure 2. Optimization of mOpto-T7RNAP in HEK293T cells. (a) Screening through different light conditions using several programs in which the duty cycle duration was changed. Illumination was done for 24 h in saturating conditions. 2:1 ratio of nMag:pMag was used. Cells were measured at the flow cytometer 24 h from illumination. (b) Screening with different light durations. Cells were measured at the flow cytometer after 48 h from transfection. Light was used in saturation regime. (c) Screening through different magnets ratios. Displayed is the reporter activation after 24 h of constant light illumination under saturating light conditions. Cells were measured at the flow cytometer. (d) Characterization of mOptoT7 with NES (nuclear export sequence) and NLS (nuclear localization sequence). Reporter expression was measured at the flow cytometer after 24 h of constant light illumination and shows that mOptoT7 can efficiently transcribe both in the nucleus and in the cytoplasm. (e) Left: Schematics of the constructs used in this experiment. Right: fluorescence images of mOptoT7 subunits with NES and NLS fused to mOrange2 and miRFP670. Images were taken after 24 h of illumination. Hoechst 33342 was used to label the nucleus. Scale bar, 20 μm. L = light, D = dark. Flow cytometry data are normalized to the constitutively expressed mCitrine. Saturating light = 400 μW/cm^2.

https://doi.org/10.1021/acssynbio.2c00067
ACS Synth. Biol. 2022, 11, 2650−2661

synthetic systems to be decoupled from cellular transcription regulation mechanisms.[16−19] This polymerase, which originates from the T7 phage, can transcribe RNA at a very high level and works orthogonally to the cellular machinery for transcription, making synthetic circuits that use it more robust and predictable, as suggested by Segall-Shapiro et al. and Shis and Bennett.[17,18] The T7 RNA polymerase only uses Mg^{2+} ions and nucleotides to carry out its function in bacteria and during *in vitro* reactions.[20] Thus, we hypothesized that the same properties apply in mammalian cells *in vivo*, making it independent from the cellular polymerase and transcription factors (thus being transcriptionally orthogonal for the expression of the reporter gene). Despite few attempts to use T7 RNA polymerase in mammalian cells both constitutively or induced by chemicals,[21−27] no optogenetic systems based on this polymerase are currently available, and no studies exist on how it impacts genetic burden.

Here we implement, characterize, and optimize a new optogenetic tool in mammalian cells (mOptoT7) that is based on a previously published optogenetic system in bacteria.[16] This tool consists of a split T7 polymerase coupled to photoregulators called Magnets,[28,29] which heterodimerize upon blue light exposure and return to monomers in the dark. mOptoT7 can carry out its function both in the cytoplasm and in the nucleus (Figure 1a),[24] and has the unique characteristic of being orthogonal to the cellular machinery for transcription. Furthermore, due to its viral origin, mOptoT7 generates RNA species that are not normally present in mammalian cells and that lack regulatory sequences at both the 3′ and 5′ end. By exploiting this feature, we optimize mOptoT7 expression level to reach a maximum of almost 20-fold change induction over the dark control. We demonstrate that mOptoT7 can be used to generate different responses in HEK293T cells, making it an ideal tool for applications where light induction and orthogonality are desired. In particular, we induced mRNA and shRNA production for protein expression and inhibition, respectively, and Pepper RNA aptamer for RNA visualization. Finally, we showed that, by being transcriptionally orthogonal, mOptoT7 can be used to reduce gene expression burden compared to another optogenetic tool.

RESULTS

Characterizing mOptoT7 in Mammalian Cells. To build a light-inducible system that can function orthogonally to the transcription machinery of mammalian cells, we implemented an optogenetic tool based on a split T7 RNA polymerase fused to the Vivid (VVD) derived Magnet photodimerization system (Opto-T7RNAPs) previously described in bacteria.[16] In the presence of blue light, the Magnets dimerize and recognize each other due to electrostatic interactions,[28] which leads to the reconstitution of the full, active protein. We tested different versions of the split T7 polymerase and found that these did not function better than the previously published split T7 in terms of fold change (Supplementary Figure S1). We, therefore, proceeded with the published split site at the amino acid position 563 and created two separate vectors containing T7(1−563) fused to nMag and T7(564−883) fused to pMag under the control of EF1α promoter, which we call mOptoT7. We built a reporter construct containing a full T7 promoter[33] to trigger the expression of mRuby3 and assess the functionality of our optogenetic tool. Due to the viral nature of the T7 polymerase, RNAs produced by the polymerase lack a 5′cap for translation initiation. To allow for initiation of translation, an IRES2 (Internal Ribosome Entry Site type 2) sequence was added between the promoter and the gene of interest (Figure 1b). We started with the characterization of the system in HEK293T cells by measuring the level of mRuby3 after 24 h of constant blue light illumination. We used a previously published[30] Light Plate Apparatus (LPA), that we optimized for our illumination experiments in mammalian cell culture conditions (see Materials and Methods section and Supplementary Figure S2). Light activation led to an 8-fold increase in fluorescence compared to the dark control (Figure 1c). Cell viability was not affected by the light conditions during the experiment as shown by Calcein AM assay. (Supplementary Figure S3).

We next investigated the response of mOptoT7 to different light intensities. Reporter fluorescence was measured in the whole population after 24 h of light illumination using flow cytometry. As was previously observed in the bacterial T7 RNAP,[16] the cells showed a graded response to light (Figure 1d).

Compared to some other available blue light systems tested with our setup,[34,35] mOptoT7 shows a higher sensitivity to light, making it an ideal system to use when low light is required for saturating gene expression. To visualize single cell gene expression variability in response to light, we imaged HEK293T cells after 24 h of constant light illumination, just before flow cytometry measurements (Figure 1e, Supplementary Figure S4). Compared to the dark control, we saw an increased mRuby3 fluorescence, which also shows a larger heterogeneity. This heterogeneity is likely due to transient transfection effects,[36] but a different degradation rate of the mOptoT7 and/or the reporter between cells cannot be excluded.[37,38] mRuby3+ population showed a relatively wide distribution, with some cells expressing a very high level of mRuby3 (Figure 1f). Integration of mOptoT7 in the genome using piggyBac transposase did not result in any activation (data not shown). This is probably due to the inhibition of mOptoT7 initiation and elongation as described previously.[25,39]

Optimization of the Mammalian OptoT7 System. An important advantage of optogenetic systems is the ability to tune gene expression through different light inputs. To test if we can control the levels of mRuby3 using mOptoT7, we performed a screen with different light programs over 24 h illumination period; we also performed a screen with different durations of the light pulse applied, always using a saturating light intensity (Figure 2a and 2b). Measurements were taken using a flow cytometer. As expected, we observed an increase in the activation of fluorescence that is proportional to the increase of light duration in the cycle, with maximal expression reached under constant light (Figure 2a). We also observed a change in mRuby3 expression when a different duration of light is applied. In particular, the system starts showing light activation with a 3 h light pulse and changes its response proportionally to the duration of pulses applied (Figure 2b).

In addition to using different light input durations, we sought to exploit the ability to change the ratio of the mOptoT7 fusion proteins during transient transfection experiments (Figure 2c). We observed a variation in both expression level and fold change with changing pMag-/nMag-fusion ratios. In particular, the highest expression level was obtained using 1:1 ratio of the magnets and the highest fold change

https://doi.org/10.1021/acssynbio.2c00067
ACS Synth. Biol. 2022, 11, 2650−2661

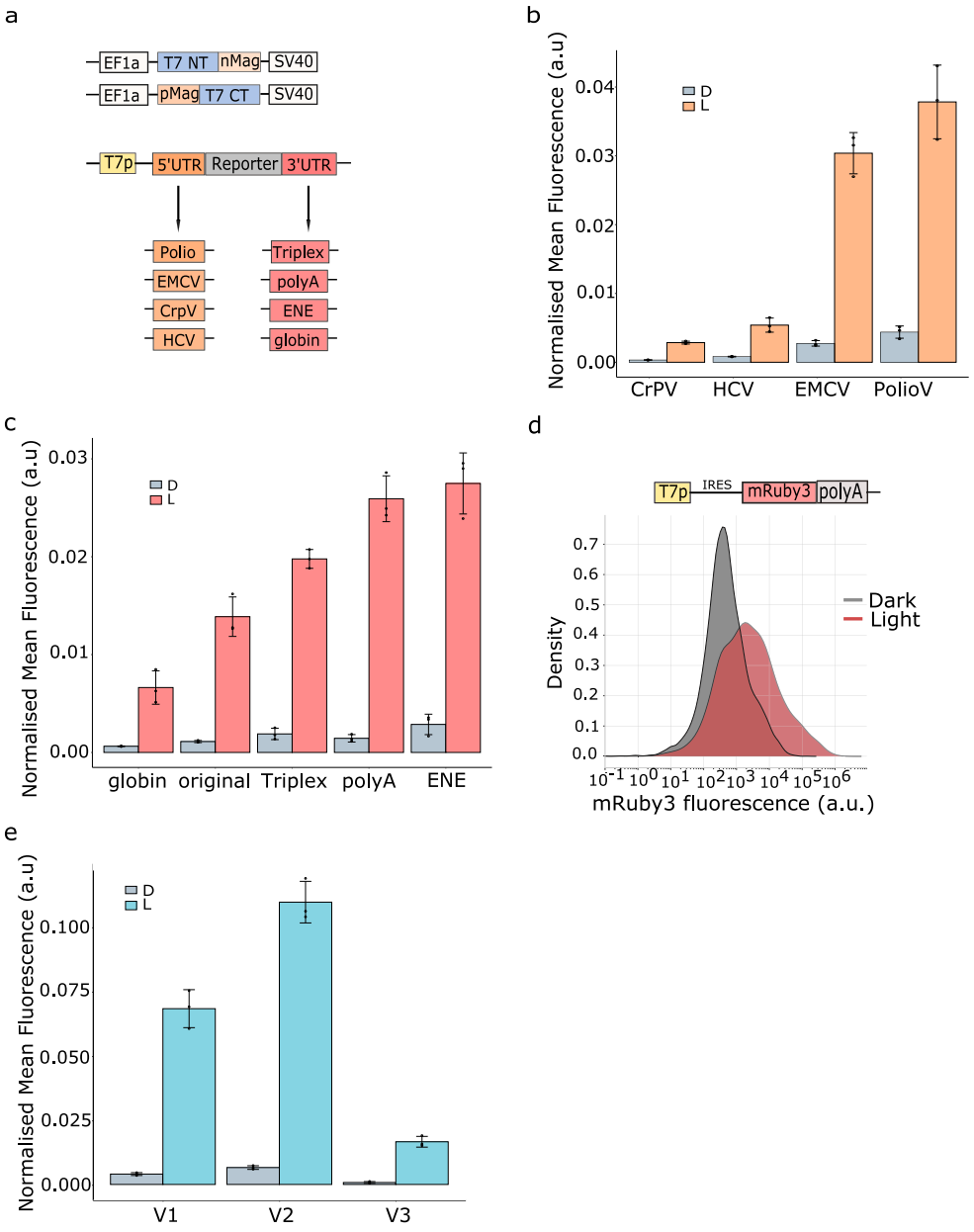

Figure 3. mOptoT7 fine-tuning: 3′ and 5′ UTR modifications. (a) Experimental design. mOptoT7 is transfected in HEK293T cells together with reporters containing one or more 5′ (shown in orange) and 3′ (shown in red) UTR modifications. (b) Testing of 5′ UTR modifications shows different expression levels for different IRES sequences. CrPV = Cricket paralysis virus; HCV = Hepatitis C virus; EMCV = encephalomyocarditis virus; PolioV = Polio virus. (c) Testing of 3′ UTR modifications. Globin = 3′ UTR from human globin gene; original = no 3′ UTR modification; triplex = RNA triple-helical structure; polyA = synthetic poly(A) stretch; ENE = element for nuclear expression. (d) Kernel density estimation plot of mRuby3 expression with the optimized version of mOptoT7 (V2). HEK293T cells were transfected with mRuby3-polyA reporter construct and measured after 24 h of constant blue light in saturating conditions. (e) New mOptoT7 versions. V1 = original design; V2 = codon optimized version; V3 = shorter 5′ UTR sequence. V2 shows the highest expression level, while V3 shows tight light response in saturating conditions. For all experiments, measurements were taken at the flow cytometer after 24 h of constant illumination in saturating conditions. Data are normalized to the constitutively expressed mCitrine. Saturating light = 400 μW/cm^2. D = dark; L = light.

compared to dark control with an excess of pMag-fusion (5:1). This last finding is consistent with investigations about OptoT7 in bacteria in which an increased expression of the pMag-fusion shows the highest light-induced fold change.[16] Ratiometric control over pMag and nMag levels can thus be used for further fine-tuning of the mOptoT7 system.

Given the viral origin of the T7 polymerase, mOptoT7 is orthogonal to the cellular machinery for transcription. To execute its function, mOptoT7 only requires nucleotides, Mg(2+) ions, and a DNA template, components that can be found both in the nucleus and in the cytoplasm.[24] In particular, during transient transfection experiments, plasmids containing the DNA template can be found both in the cytoplasm and in the nucleus allowing the T7 polymerase to perform its function in both these compartments.[41] We hypothesized that mOptoT7 will be able to transcribe RNA very efficiently outside of the nucleus, allowing a complete separation of transcription activities from the endogenous cellular transcription, and at the same time concentrating mRNA directly in the cytoplasm. To test if mOptoT7 can indeed function

https://doi.org/10.1021/acssynbio.2c00067
ACS Synth. Biol. 2022, 11, 2650−2661

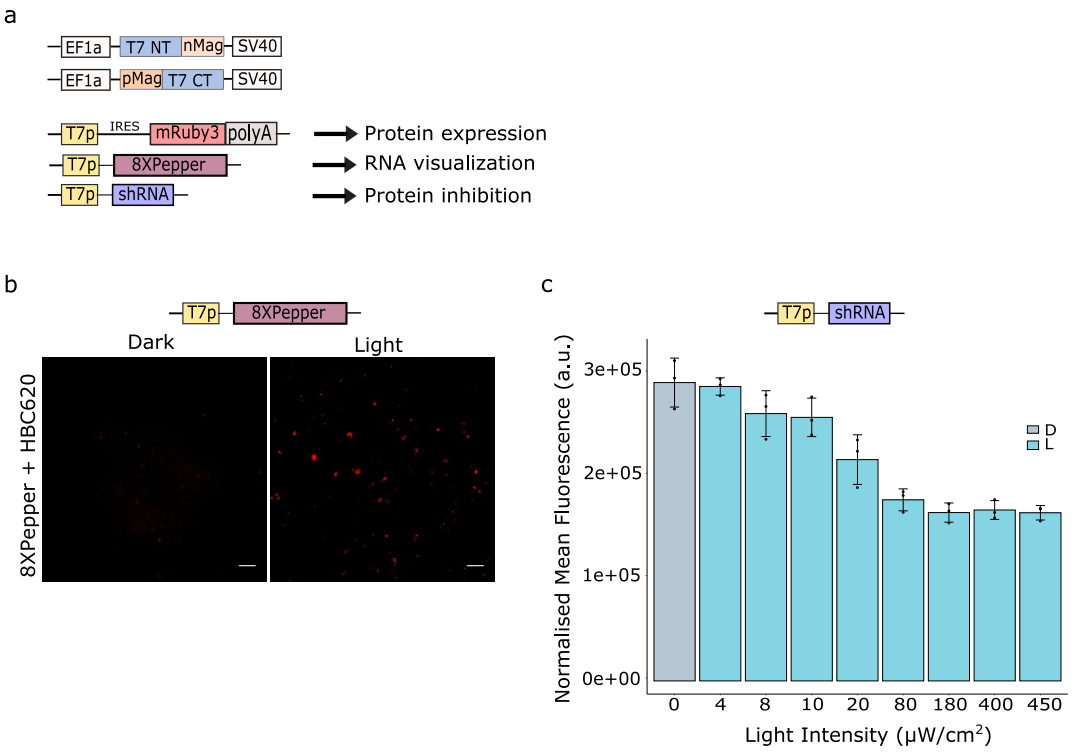

Figure 4. Protein expression/inhibition and RNA visualization with mOptoT7. (a) Design of the mOptoT7 vectors for gene expression, inhibition, and RNA visualization. (b) Testing of the mOptoT7 plasmid with a fluorescent RNA aptamer (8XPepper) as the output. Images were taken after 30 h of constant blue light illumination in saturating conditions. Scale bar, 50 μm. (c) Flow cytometry results of the mOptoT7 vector with shRNA targeting mCitrine as the output. Cells were measured after 24 h of constant blue light illumination. Data are normalized to the constitutively expressed mCitrine. Saturating light = 400 μW/cm^2.

within and outside the nucleus, we introduced either a strong nuclear localization sequence (NLS) or a strong nuclear export sequence (NES) before both subunits of the mOptoT7 and compared the activities of these constructs with the original ones without NLS/NES by the measuring mRuby3 fluorescence after 24 h of blue light illumination in saturating conditions (Figure 2d). We observed that fluorescent protein expression levels did not significantly change between the two variants, supporting the conclusion that mOptoT7 can transcribe RNA directly and efficiently in the cytoplasm. To investigate if a small fraction of mOptoT7 still present in the nucleus is responsible for the observed reporter expression, we performed a control experiment in which we titrated the mOptoT7 plasmid amount. As expected, the expression level of the reporter plasmid decreased correspondingly with the decreasing of the total amount of mOptoT7 plasmid used during transfection (Supplementary Figure S5). To confirm the localization of the mOptoT7 in the different cellular compartments, we next fused a fluorescent protein (either mOrange2 or miRFP670) to each of the mOptoT7 subunits, and imaged the fluorescence at the microscope 48 h after transfection (Figure 2e). Supporting our previous results, we observed a strong nuclear or cytoplasmic localization for the variants with NLS and NES sequences respectively, while the mOptoT7 without any localization sequence localized in the whole cell (Supplementary Figure S6). We did not observe a change in localization after shining constant blue light for 24 h nor did we observe significant changes when the fluorescent proteins were switched between the two subunits for the conditions tested (Supplementary Figure S6).

Fine-Tuning of mOptoT7: Exploiting T7 Polymerase Viral Origin. As previously mentioned, the T7 polymerase generates RNA transcripts that lack 5′ and 3′ UTR modifications. These modifications are essential in controlling translation initiation and increasing RNA stability.[40,42] Without them, RNA transcripts will not be translated and RNA half-life will be short. Thus, to further fine-tune mOptoT7-mediated reporter expression, we created new variants of the mOptoT7 by changing 5′ and 3′ UTR sequences independently (Figure 3a).

Inspired by the different strategies that viruses have evolved to initiate translation and stabilize RNA in mammalian cells, we designed new reporter constructs containing IRES sequences from different type of viruses, (i) PolioV-IRES (IRES1), (ii) EMCV-IRES (IRES2), (iii) HCV-IRES (IRES3/4), and (iv) CrpV-IRES (IRES4), upstream of mRuby3 (Figure 3a) and measured fluorescence after 24 h of light illumination (Figure 3b). These sequences are categorized in four different types according to RNA structure and eIFs (eukaryotic initiation factors) recruitment, with type 1 being the most complex and recruiting most factors and type 4 having a simple structure and binding directly to ribosomal subunits for translation initiation.[43,44] We hypothesized that by recruiting different eIFs, IRES sequences can be used to generate different expression levels of mOptoT7 reporter construct. We indeed observed that these structures can titrate different expression levels of mRuby3. Maximum expression was obtained using PolioV-IRES, while the lowest expression was obtained using CrPV-IRES. In particular, due to their simplistic structure and ability to initiate translation with only few translation elongation factors (eIFs), CrPV- and HCV-

https://doi.org/10.1021/acssynbio.2c00067
ACS Synth. Biol. 2022, 11, 2650−2661

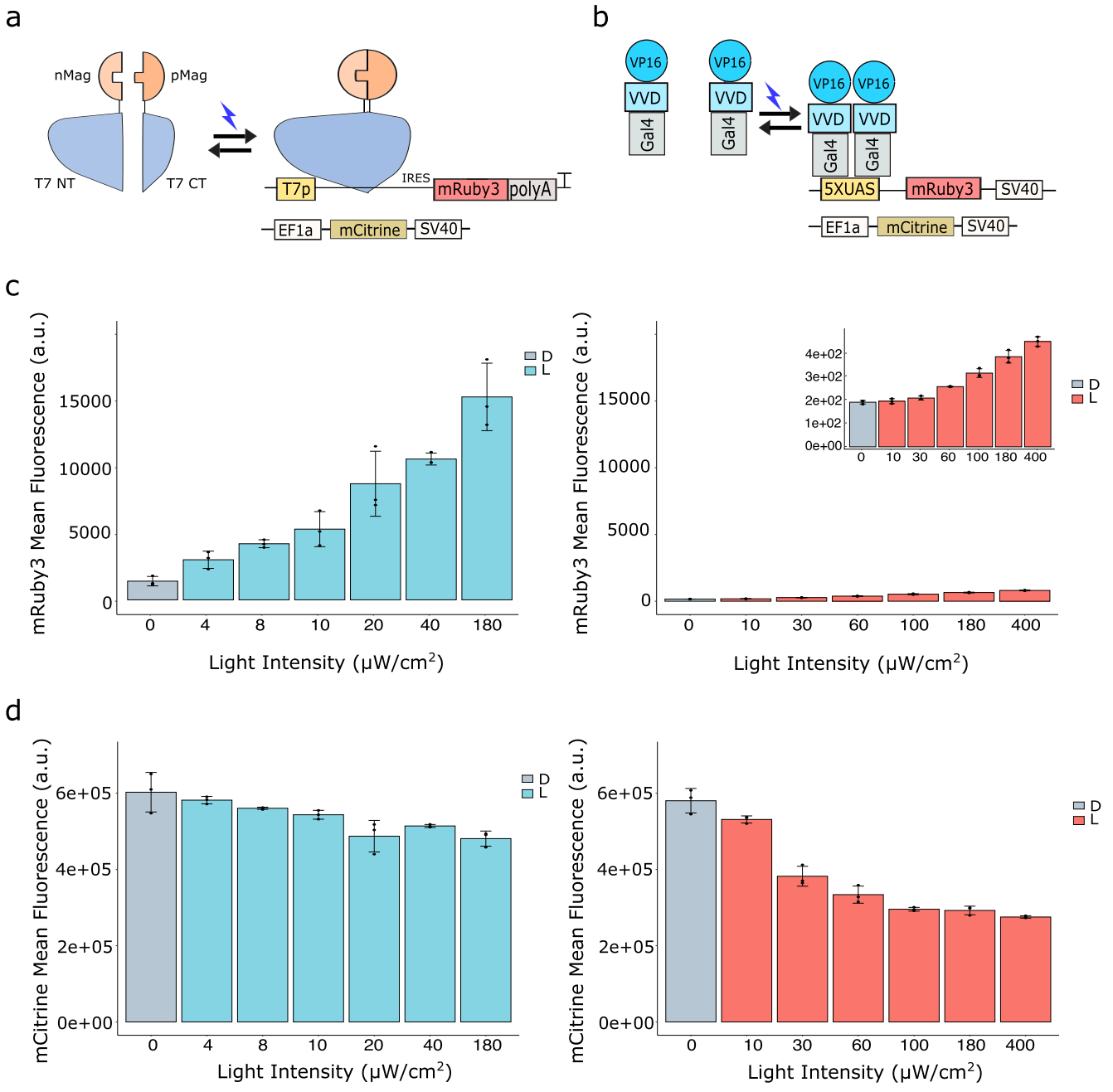

Figure 5. mOptoT7 reduces burden in HEK293T cells. (a,b) Schematics of mOptoT7 and GAV-VP16 used in this experiment. mRuby3 fluorescent protein was used as reporter color. mCitrine under the control of EF1a promoter was used as constitutive color (capacity monitor). (c) Dose response of mOptoT7 (left panel) and GAV-VP16 (right panel) reporter to increasing light intensity. Data represent the mean of mRuby3 in transfected cells with either mOptoT7 and GAV-VP16 in dark and light conditions. (d) Capacity monitor's response to increasing light intensity for mOptoT7 (left) and GAV-VP16 (right) shows less reduction in the expression of mOptoT7 capacity monitor compared to GAV-VP16. D = dark, L = light. Measurements are taken after 24 h of constant blue light illumination.

IRES could be of interest for applications that do not require the use of all cellular resources for translation.

Next, we focused on 3′ UTR modifications. In eukaryotic cells, endogenous RNA is made bearing 3′ UTR modifications in the form of a poly(A) stretch. This repetition of (A)s is correlated with RNA stability, and transcripts that lack poly(A) tails are known to be short-lived.[45] With the aim of increasing RNA stability and thus mRuby3 expression in our mOptoT7 reporter, we created constructs that contain different stabilizing sequences at the 3′ region of mRuby3: (i) a triple RNA helix (triplex) that, as described previously,[46] is used to stabilize noncoding RNAs; (ii) a long stretch of synthetic poly(A)s to mimic the natural occurring adenylation process; (iii) an element for nuclear expression (ENE) that, as described previously,[47] is used to stabilize poly(A) transcripts by sequestrating them in triple helix structures; or (iv) the 3′ UTR of the globin gene, which is known to be rather stable[48] (Figure 3a). We observed that we could indeed tune reporter expression levels in a wide range after 24 h of light illumination by changing the 3′ UTR sequence of the mRuby3 reporter,

https://doi.org/10.1021/acssynbio.2c00067
ACS Synth. Biol. 2022, 11, 2650−2661

with maximum expression obtained using the element for nuclear expression (ENE), and the lowest expression using the 3′ UTR of the globin gene (Figure 3c). Interestingly, the addition of a poly(A) tail not only increased mRuby3 expression, but also increased the total population that was responsive to light (Figure 3d and Supplementary Figure S7).

Finally, we aimed to create versions of the mOptoT7 that not only had higher light-induced expression levels, but also showed reduced leakiness, as an ideal optogenetic system should satisfy both of these criteria. Thus, we first created codon optimized versions of the magnets (V2) that, when combined with the reporter containing the synthetic poly(A) tail, gave around 20-fold change, low background activity, and the highest expression (Figure 3e) compared to the noncodon optimized version (V1). Induction of mRuby3 reporter fluorescence with our optimized mOptoT7 version (V2) showed the highest fluorescent protein expression as well as the highest percentage of cells responding to the light input (Figure 3d). Almost 50% of the population activates mRuby3 production after illumination compared to only 15% using the construct before optimization (Supplementary Figure S7). We then created another version (V3) by modifying the length of the 5′ UTR region of the optimized mOptoT7 polymerase fusion proteins. We hypothesized that the length and composition of 5′ UTR sequence will affect transcription rate and RNA stability. Indeed, we found that by decreasing the number of nucleotides between the constitutive EF1α promoter and the start of each subunit of the mOptoT7, we were able to change its transcription and therefore protein availability, to create a very tight gene expression system. When light is applied, this version shows 10-fold change with saturating light and no measurable background activity (V3, Figure 3e). This last system is to be preferred in applications for which tight control in the dark is essential while high expression is not required.

mOptoT7 Can Be Used to Visualize RNA and Inhibit Gene Expression. We next assessed the ability of mOptoT7 to generate two more outputs apart from gene expression for a wider range of applications: (i) RNA production for visualization, and (ii) inhibition of gene expression (Figure 4a). Both RNA visualization and gene expression inhibition were previously shown using T7 polymerase in mammalian cells,[21] but without the opportunity for dynamic control that is enabled by optogenetics. For our experiments, we created one vector containing both subunits of the mOptoT7 so that we could easily use the 1:1 ratio of the mOptoT7 fusion proteins that showed the highest expression level.

The ability of mOptoT7 to produce RNA species without 5′ and 3′ UTR can be exploited to generate hairpin repeats that can be visualized after binding with fluorophores or used in downstream applications. Thus, we next used a Pepper RNA aptamer (8 repeats) under the control of the T7 promoter to visualize RNA production using the mCherry fluorophore-like synthetic dye HBC620.[32] RNA production is detected after 24 h of constant light illumination, while the dark control shows no signal (Figure 4b). Nontransfected cells stained using HBC620 show no expression (Supplementary Figure S8a). Cells expressing 8xPepper constitutively in the presence or absence of light showed a uniform distribution of RNA within the cell population, and mainly in the cytoplasm (Supplementary Figure S8b). Interestingly, cells exhibited different patterns of RNA expression, with some cells expressing many RNA molecules homogeneously diffused and others expressing RNA in the form of "dots". This difference in expression is likely due to different plasmid uptake during transient transfection experiments.

Finally, we wanted to investigate if we can also use mOptoT7 to inhibit gene expression. Therefore, we made another vector containing an shRNA hairpin[49] against mCitrine under the control of the T7 promoter. We transfected cells with this construct together with the mOptoT7 and a constitutive mCitrine plasmid and measured the expression of mCitrine in response to 24 h light exposure at different intensities (Figure 4c). We observed that the fluorescent signal decreased with increasing light intensity, reaching almost 50% of the mCitrine fluorescence levels in the dark. These results show that mOptoT7 can also be used to inhibit gene expression through a polymerase that is orthogonal to the cellular one, highlighting the potential for the use of mOptoT7 for research questions on gene function.

mOptoT7 Shows Reduced Burden on the Host Cell. Finally, we wanted to assess the ability of mOptoT7 to avoid gene expression burden that is commonly exerted by other optogenetic tools that rely on the recruitment of the cellular polymerase. Given the orthogonality of mOptoT7 in generating RNA transcripts (transcriptional orthogonality) (Figure 2d), we hypothesized that mOptoT7 will use less overall cellular resources (e.g., polymerase subunits, eIFs), thereby imposing less burden to the cell. This effect, if present, could be seen downstream of gene production, by measuring protein expression levels.

To test this, we used mOptoT7 together with the reporter bearing the IRES2 sequence and a poly(A) tail to have high expression level of mRuby3. To measure the effect of increasing mRuby3 expression level in response to light, we used a "sensor gene" called capacity monitor as previously described.[8] In our case, the capacity monitor consisted of mCitrine fluorescent protein under the control of EF1α promoter (Figure 5a). As comparison, we used another VVD-based optogenetic tool, called GAVPO.[50] Given that GAVPO has a stronger reporter expression with light compared to mOptoT7, we replaced the p65 activation domain with the weaker activation domain VP16,[51] thus making the two systems more comparable (Figure 5b). In response to increasing light intensity, we observed an increase in reporter expression for both mOptoT7 and GAV-VP16, with the latter having a weaker mRuby3 expression level (Figure 5b). Interestingly, when looking at the capacity monitor for both systems, we clearly saw a sharper decrease in mCitrine expression level with increasing light intensity when using GAV-VP16, despite having a weaker expression level for the reporter (Figure 5c, right) compared to the mOptoT7 reporter expression (Figure 5c, left). This supports our hypothesis that mOptoT7 can be used to minimize gene expression burden. We then tested whether we could see a stronger effect on burden if a reporter that does not require translational resources was used. For this, 8XPepper aptamer, used for RNA visualization, was cloned downstream of mOptoT7 and GAV-VP16's promoters, respectively. In response to increasing light intensity, we observed an increase in RNA transcription for mOptoT7, but not for GAV-VP16. Interestingly, when looking at the capacity monitor, we clearly saw a decrease in mCitrine expression level with increasing light intensity for GAV-VP16, but not for mOptoT7 (Supplementary Figure S9 and Supplementary Figure S10b,c). This further confirms that mOptoT7 can be used to reduce gene expression burden

https://doi.org/10.1021/acssynbio.2c00067
ACS Synth. Biol. 2022, 11, 2650−2661

compared to GAV-VP16. We hypothesize that GAV-VP16 produced very low RNA compared to mOptoT7 and therefore could not be detected using 8XPepper aptamer. However, the amount produced was sufficient to create a burden on the cell. This hypothesis is supported by the fact that a strong EF1α driven 8XPepper plasmid also showed a weaker signal compared to mOptoT7 (Supplementary Figure S10a). To exclude the possibility that blue light causes this effect, we shined an increasing amount of light on cells transfected only with the capacity monitor and measured their expression level after 24 h from illumination. No decrease in mCitrine levels was observed at the applied light intensities (Supplementary Figure S11).

DISCUSSION

In this study we created mOptoT7, a novel optogenetic tool in HEK293T cells based on a split T7 RNA polymerase coupled with the light-responsive magnet dimers derived from VVD.[16] This is the first time that an optogenetic system orthogonal to the cellular transcriptional machinery is applied in mammalian cells. mOptoT7 can activate downstream gene expression upon light exposure with almost 20-fold change over the dark control and relatively low leakiness (Figure 3e). By changing the 5′ and 3′ UTR ends of the RNA species generated, we were able to fine-tune mOptoT7 reporter expression creating a wide range of induction responses. The addition of poly(A) tails at the 3′ UTR of the reporter construct increased not only the expression level, but also the number of cells that were activated after illumination (Figure 4b and Supplementary Figure S7). We showed that mOptoT7 can produce high amounts of RNA when compared to a constitutive promoter (Supplementary Figure S9 and S10); however, the protein expression level is low. Therefore, further studies on optimizing the system should focus on RNA stability and/or translation efficiency.

While we observed heterogeneity in reporter gene expression upon light activation of mOptoT7, this is not unlike other optogenetic tools, especially during transient transfection experiments.[35,36,52] On a more general level, little is known about the way optogenetic systems affect cellular functions or how they are affected by cellular state and metabolic stress, complicating their robust use in different cell lines and conditions.[53,54] Future work should focus on solving some of these problems.

We showed that mOptoT7 can efficiently transcribe RNA both in the cytoplasm and in the nucleus, confirming the independence of the polymerase from transcriptional resources located in the nuclear compartment. This property is particularly relevant when compartmentalization of RNA is desired. Battich et al. showed that nuclear retention of RNA can filter out noise and explain transcriptional bursts in mammalian cells.[55] However, until now, no system is available to investigate and potentially control how the noise distribution is affected by RNA production in different compartments, which could also have an application in building synthetic cells.[56]

The capability of mOptoT7 to transcribe RNA in the cytoplasm is connected to its orthogonality to the cellular machinery. This property is especially interesting if applied to studying resource allocation and gene expression burden. Recently, several studies have shown how burden in mammalian cells is generated through the sharing of cellular resources both at the transcriptional and translational level.[8,9] The ability to isolate exogenous genes from the cellular resources can be used, for example, in bioproduction where the stable generation of a protein over time can have dramatic consequences on its yield and downstream applications.[59] We showed that using mOptoT7 to orthogonally generate RNA species (in an inducible manner) not only helps in reducing burden, but can also help in gaining a better understanding of the effect of transcriptional resources on burden as a whole. In this context, the contribution of IRES sequences that are included in the mOptoT7 reporter are not considered in this study and require further investigation. Complete independence from the cellular machineries is extremely challenging to achieve; however, we showed that decoupling the transcriptional expression of an inducible gene can be enough to reduce burden on the cell. As such, mOptoT7's ability to reduce fluctuations in gene expression (which may arise due to burden) can support efforts to make genetic circuits and optogenetic experiments more reliable.

Besides orthogonality, another interesting feature of mOptoT7 is its ability to generate transcripts that lack endogenous RNA modifications. In this study we visualize the localization of these transcripts using Pepper RNA aptamers. Interestingly, we see a mixed response in RNA production, with some cells showing "dot-like" structures located mostly around the nucleus. These aggregates could be virus-induced RNA granules (stress granules) that are formed in response to a viral infection and can inhibit translation.[57,58] Potentially, disruption of these granules could further increase mOptoT7 reporter expression level. However, this remains a theory at this point. As such, mOptoT7 could be employed to study viral RNA recognition and degradation in mammalian cells.

Studies in bacteria have shown how the T7 RNA polymerase can be used to create more robust and stable genetic circuits.[17,60] The ability of mOptoT7 to be induced with light, as well as the diversity of available T7 variants, can be used as powerful tool to create synthetic networks with different feedback and feedforward properties. These genetic circuits can be used for cell-based therapies and clinical applications where stability and reliability play an important role.

To conclude, in this study we implemented, characterized, and optimized a new optogenetic tool in mammalian cells. mOptoT7 has some unique features that are not shared by any other optogenetic tool currently available. The orthogonality to the cellular machinery and the viral RNA origin can be exploited both in synthetic biology and basic science to gain a better understanding of gene expression processes in mammalian cells.

MATERIALS AND METHODS

Cell Culture and Transfection. HEK293T cells (ATCC, strain number CRL-3216) were cultured in Dulbecco's modified Eagle medium (DMEM, Gibco) supplemented with 10% FBS (Sigma-Aldrich), 1% penicillin/streptomycin, 1× GlutaMAX (Gibco) and 1 mM Sodium Pyruvate (Gibco). Cells were kept at 37 °C and 5% CO_2. Transfections were performed in a 24 well black plate (PerkinElmer) format for flow cytometry. Cells were seeded in 24 well plates at a density of 8×10^4 cells/well 1 day before transfection or at 1.6×10^5 for transfections done in suspension. HEK293T were transfected with Polyethylenimine (PEI) (Mw 40 000; Polysciences, Inc.) using a ratio of 1:3 (μg DNA to μg PEI) with a total of

https://doi.org/10.1021/acssynbio.2c00067
ACS Synth. Biol. 2022, 11, 2650−2661

500 μg of DNA/well for 24 well plates. If not otherwise indicated, 200 ng/well of the T7 plasmid and 275 ng/well of the reporter plasmid was used. OptiMEM I reduced serum media (Gibco) was used to separately dilute both DNA and PEI. Once mixed, DNA and PEI were incubated for 20 min at room temperature to allow complexes formation prior to addition to the cells. After transfection, cells were kept in the dark for approximately 24 h before starting illumination.

Light Induction. For flow cytometry measurements, cells were illuminated with 470 nm LEDs (Super Bright LEDs Inc.) using a modified version of the Light Plate Apparatus (LPA) previously described.[30] The LPA was modified by adding a 2 cm aluminum heatsink and a ventilator both connected to the PCB in order to improve heat dissipation. In addition, a second adaptor and 2 layers of filter papers were added to allow a uniform distribution of light (Supplementary Figure S2). Cells were illuminated with constant or pulsed light (of different duration) as stated in the specific experimental conditions. The intensity of light received by the cells was measured to be 400 μW/cm2 at saturation using the S175C—Microscope Slide Thermal Power Sensor from ThorLabs. The control plate was kept in the dark during the entire experiment.

Flow Cytometry Analysis. HEK293T cells were analyzed with CytoFLEX S Flow Cytometer (Beckman Coulter) after 24 h or 48 h of illumination and using 488 and 561 lasers with 530/11 nm and 610/20 nm OD1 bandpass filters, respectively. Prior to measurement, cells were washed once with DPBS (Thermo Fisher) and incubated with 100 μL of Accutase solution (Sigma-Aldrich) to allow detachment. For each sample, FCS/SSC parameters were used to select the main population of cells and singlets. When necessary, a compensation matrix was made using single color controls and untransfected cells (Supplementary Figure S7). In every experiment, >20 000 events were collected for each sample, and data analysis was done using Cytoflow Software and a customized R code.

Plasmid Construction. All plasmids were constructed using standard restriction digestion cloning or using Golden Gate assembly and a previously described[31] yeast toolkit (YTK) with customized parts for use in mammalian cells. In the standard cloning, PCR amplifications were performed using Phusion Flash high fidelity DNA polymerase (Thermo-Fisher Scientific), and ligation reactions were made using 1:3 ratios of vector plasmid:insert and incubation time of 1 h at room temperature. All constructs were chemically transformed into TOP10 *E. coli* cells and checked through sequencing (Microsynth). All relevant plasmid sequences can be found in the Supporting Information.

Live-Cell Imaging. A Nikon Ti2e inverted microscope (Nikon Instruments) equipped with an ORCA Flash4.0 LT+ camera and a chamber for CO_2 and temperature regulation was used. Cells were always kept at 37 °C and with 5% CO_2. Cells were imaged after 24 to 72 h from transfection with constant illumination (performed after 24 h from transfection) or after being in the dark for the same amount of time. For all experiments, mRuby3/mOrange2, mCitrine and miRFP670 fluorescence was imaged using NIS element software and with 561/4, 543/22, and 692/40 filters, respectively (BrightLine HC). CFI Plan Apochromat Lambda 10× (N.A. 0.45, W.D. 4.0 mm), CFI S Plan Fluor ELWD 20XC (N.A. 0.45, W.D. 8.2–6.9 mm), or CFI S Plan Fluor ELWD 40XC (N.A. 0.6, W.D. 3.6–2.8 mm) were used. For brightfield imaging, LED 100 (Märzhäuser Wetzlar GmbH & Co. KG) was used. Here, a diffuser and a green interference filter was positioned in the light path. Image analysis was done with ImageJ software. Hoescht 33342 staining (ThermoFisher) was used to label the nucleus according to manufacturer's instructions.

RNA Visualization. RNA in live cells was visualized using Pepper RNA aptamer as previously described.[32] Eight times Pepper repeats were cloned downstream of the T7 promoter, and their expression was driven with light starting 24 h after transfection. After 30 h of illumination, cells were stained using 20 μM of HBC620 (FR Biotechnologies) supplemented with 5 mM of $MgSO_4$. Cells were incubated for 30 min at 37 °C with 5% CO_2 and then transferred to the microscope for imaging. When used for flow cytometry, cells were detached and incubated for 30 min at RT with 1×PBS/4% FBS buffer containing 0.5 μM of HBC620 (Lucerna-Chem) supplemented with 5 mM of $MgSO_4$.

Viability Assay. Cells were stained using Calcein AM (Sigma-Aldrich) dye after 24 h of blue light illumination at different intensities. Cells were prepared for flow cytometry analysis as described previously. Thirty minutes before measurements, Calcein AM was added to the cells at 1 μM final concentration. Samples were incubated on ice until measurement.

Statistics. Each experiment was repeated with at least three independent biological replicates, from which mean and standard deviation are calculated.

■ ASSOCIATED CONTENT

Supporting Information

The Supporting Information is available free of charge at https://pubs.acs.org/doi/10.1021/acssynbio.2c00067.

Additional information; light setup design; control experiments; plasmid maps; flow cytometry gating; raw data (PDF)

■ AUTHOR INFORMATION

Corresponding Author

Mustafa Khammash − *Department of Biosystems Science and Engineering, ETH Zürich, 4058 Basel, Switzerland*; Email: mustafa.khammash@bsse.ethz.ch

Authors

Sara Dionisi − *Department of Biosystems Science and Engineering, ETH Zürich, 4058 Basel, Switzerland*; orcid.org/0000-0001-5735-780X

Karol Piera − *Department of Biosystems Science and Engineering, ETH Zürich, 4058 Basel, Switzerland*

Armin Baumschlager − *Department of Biosystems Science and Engineering, ETH Zürich, 4058 Basel, Switzerland*; orcid.org/0000-0002-2546-9038

Complete contact information is available at: https://pubs.acs.org/10.1021/acssynbio.2c00067

Author Contributions

S.D. conceived the study, performed experiments, analyzed data, and wrote the paper. A.B. helped conceive the study, co-supervised K.P., and reviewed the manuscript. K.P. created the original reporter vector and performed initial characterization experiments. M.K. supervised the study, reviewed the manuscript, and secured funding.

Notes

The authors declare no competing financial interest.

https://doi.org/10.1021/acssynbio.2c00067
ACS Synth. Biol. 2022, 11, 2650−2661

All relevant data are included and are available from the corresponding author. Strains and plasmids used in this study are available from the corresponding author upon reasonable request. Main plasmid maps used can be found in the Supporting Information.

■ ACKNOWLEDGMENTS

We thank Peter Buchmann for his help in building the LED setup, and Dr. Stephanie Aoki and Dr. Maaike Welling for their feedback on the manuscript. This project has received funding from the European Research Council (ERC) under the European Union's Horizon 2020 research and innovation programme (CyberGenetics; grant agreement 743269).

■ REFERENCES

(1) Chu, G. C.; Dunn, N. R.; Anderson, D. C.; Oxburgh, L.; Robertson, E. J. Differential requirements for Smad4 in TGFβ-dependent patterning of the early mouse embryo. *Development* **2004**, *131*, 3501−3512.
(2) Takahashi, K.; Yamanaka, S. Induction of Pluripotent Stem Cells from Mouse Embryonic and Adult Fibroblast Cultures by Defined Factors. *Cell* **2006**, *126*, 663−676.
(3) Qi, Z.; Li, Y.; Zhao, B.; Xu, C.; Liu, Y.; Li, H.; Zhang, B.; Wang, X.; Yang, X.; Xie, W.; Li, B.; Han, J.-D. J.; Chen, Y.-G. BMP restricts stemness of intestinal Lgr5 + stem cells by directly suppressing their signature genes. *Nat. Commun.* **2017**, DOI: 10.1038/ncomms13824.
(4) Khalil, A. S.; Collins, J. J. Synthetic biology: Applications come of age. *Nat. Rev. Genet.* **2010**, *11*, 367−379.
(5) Saxena, P.; Heng, B. C.; Bai, P.; Folcher, M.; Zulewski, H.; Fussenegger, M. A programmable synthetic lineage-control network that differentiates human IPSCs into glucose-sensitive insulin-secreting beta-like cells. *Nat. Commun.* **2016**, *7*, 11247.
(6) Weber, W.; Rimann, M.; Spielmann, M.; Keller, B.; Daoud-El Baba, M.; Aubel, D.; Weber, C. C.; Fussenegger, M. Gas-inducible transgene expression in mammalian cells and mice. *Nat. Biotechnol.* **2004**, *22*, 1440−1444.
(7) Ausländer, D.; Ausländer, S.; Charpin-El Hamri, G.; Sedlmayer, F.; Müller, M.; Frey, O.; Hierlemann, A.; Stelling, J.; Fussenegger, M. A synthetic multifunctional mammalian pH sensor and CO2 transgene-control device. *Mol. Cell* **2014**, *55*, 397−408.
(8) Frei, T.; Cella, F.; Tedeschi, F.; Gutiérrez, J.; Stan, G. B.; Khammash, M.; Siciliano, V. Characterization and mitigation of gene expression burden in mammalian cells. *Nat. Commun.* **2020**, *11*, 1−14.
(9) Jones, R. D.; Qian, Y.; Siciliano, V.; DiAndreth, B.; Huh, J.; Weiss, R.; Del Vecchio, D. An endoribonuclease-based feedforward controller for decoupling resource-limited genetic modules in mammalian cells. *Nat. Commun.* **2020**, *11*, 1−16.
(10) Weiße, A. Y.; Oyarzún, D. A.; Danos, V.; Swain, P. S. Mechanistic links between cellular trade-offs, gene expression, and growth. *Proc. Natl. Acad. Sci. U. S. A.* **2015**, *112*, E1038−E1047.
(11) Tischer, D.; Weiner, O. D. Illuminating cell signalling with optogenetic tools. *Nat. Rev. Mol. Cell. Biol.* **2014**, *15*, 551−558.
(12) Williams, S. C. P.; Deisseroth, K. Optogenetics. *Proc. Natl. Acad. Sci. U. S. A.* **2013**, *110*, 16287.
(13) Johnson, H. E.; Toettcher, J. E. Illuminating developmental biology with cellular optogenetics. *Curr. Opin. Biotechnol.* **2018**, *52*, 42−48.
(14) Baumschlager, A.; Khammash, M. Synthetic Biological Approaches for Optogenetics and Tools for Transcriptional Light-Control in Bacteria. *Adv. Biol.* **2021**, *5*, 2000256.
(15) Liu, Q.; Tucker, C. L. Engineering genetically-encoded tools for optogenetic control of protein activity. *Curr. Opin. Chem. Biol.* **2017**, *40*, 17−23.
(16) Baumschlager, A.; Aoki, S. K.; Khammash, M. Dynamic Blue Light-Inducible T7 RNA Polymerases (Opto-T7RNAPs) for Precise Spatiotemporal Gene Expression Control. *ACS Synth. Biol.* **2017**, *6*, 2157−2167.
(17) Segall-Shapiro, T. H.; Meyer, A. J.; Ellington, A. D.; Sontag, E. D.; Voigt, C. A. A 'resource allocator' for transcription based on a highly fragmented T7 RNA polymerase. *Mol. Syst. Biol.* **2014**, *10*, 742.
(18) Chamberlin, M.; Mcgrath, J.; Waskell, L. New RNA polymerase from escherichia coli infected with bacteriophage T7. *Nature* **1970**, *228*, 227−231.
(19) Kushwaha, M.; Salis, H. M. A portable expression resource for engineering cross-species genetic circuits and pathways. *Nat. Commun.* **2015**, DOI: 10.1038/ncomms8832.
(20) Ling, M. L.; Risman, S. S.; Klement, J. F.; Mcgraw, N.; Mcallister, W. T. Abortive initiation by bacteriophage T3 and T7 RNA polymerases under conditions of limiting substrate. *Nucleic Acids Res.* **1989**, *17*, 4430.
(21) Pu, J.; Zinkus-Boltz, J.; Dickinson, B. C. Evolution of a split RNA polymerase as a versatile biosensor platform. *Nat. Chem. Biol.* **2017**, *13*, 432−438.
(22) Chen, X.; Li, Y.; Xiong, K.; Wagner, T. E. A self-initiating eukaryotic transient gene expression system based on cotransfection of bacteriophage T7 RNA polymerase and DNA vectors containing a T7 autogene. *Nucleic Acids Res.* **1994**, *22*, 2114−2120.
(23) Lieber, A.; Kiessling, U.; Strauss, M. High level gene expression in mammalian cells by a nuclear T7-phage RNA polymerase. *Nucleic Acids Res.* **1989**, *17*, 8485−8493.
(24) Elroy-Stein, O.; Moss, B. Cytoplasmic expression system based on constitutive synthesis of bacteriophage T7 RNA polymerase in mammalian cells. *Proc. Natl. Acad. Sci. U. S. A.* **1990**, *87*, 6743−6747.
(25) Fuerst, T. R.; Niles, E. G.; Studier, F. W.; Moss, B. Eukaryotic transient-expression system based on recombinant vaccinia virus that synthesizes bacteriophage T7 RNA polymerase. *Proc. Natl. Acad. Sci. U. S. A.* **1986**, *83*, 8122−8126.
(26) Brisson, M.; He, Y.; Li, S.; Yang, J. P.; Huang, L. A novel T7 RNA polymerase autogene for efficient cytoplasmic expression of target genes. *Gene Ther.* **1999**, *6*, 263−270.
(27) Ghaderi, M.; Sabahi, F.; Sadeghi-zadeh, M.; Khanlari, Z.; Jamaati, A. Construction of an eGFP Expression Plasmid under Control of T7 Promoter and IRES Sequence for Assay of T7 RNA Polymerase Activity in Mammalian Cell Lines. *Iran J. Cancer Prev.* **2014**, *7*, 137−141.
(28) Kawano, F.; Suzuki, H.; Furuya, A.; Sato, M. Engineered pairs of distinct photoswitches for optogenetic control of cellular proteins. *Nat. Commun.* **2015**, *6*, 6256.
(29) Pathak, G. P.; Strickland, D.; Vrana, J. D.; Tucker, C. L. Benchmarking of optical dimerizer systems. *ACS Synth. Biol.* **2014**, *3*, 832−838.
(30) Gerhardt, K. P.; Olson, E. J.; Castillo-Hair, S. M.; Hartsough, L. A.; Landry, B. P.; Ekness, F.; Yokoo, R.; Gomez, E. J.; Ramakrishnan, P.; Suh, J.; Savage, D. F.; Tabor, J. J. An open-hardware platform for optogenetics and photobiology. *Sci. Rep.* **2016**, *6*, 35363.
(31) Lee, M. E.; DeLoache, W. C.; Cervantes, B.; Dueber, J. E. A Highly Characterized Yeast Toolkit for Modular, Multipart Assembly. *ACS Synth. Biol.* **2015**, *4*, 975−986.
(32) Chen, X.; Zhang, D.; Su, N.; Bao, B.; Xie, X.; Zuo, F.; Yang, L.; Wang, H.; Jiang, L.; Lin, Q.; et al. Visualizing RNA dynamics in live cells with bright and stable fluorescent RNAs. *Nat. Biotechnol.* **2019**, *37*, 1287−1293.
(33) Rong, M.; He, B.; McAllister, W. T.; Durbin, R. K. Promoter specificity determinants of T7 RNA polymerase. *Proc. Natl. Acad. Sci. U. S. A.* **1998**, *95*, 515−519.
(34) Kennedy, M. J.; Hughes, R. M.; Peteya, L. A.; Schwartz, J. W.; Ehlers, M. D.; Tucker, C. L. Rapid blue-light-mediated induction of protein interactions in living cells. *Nat. Methods* **2010**, *7*, 973−975.
(35) Motta-Mena, L. B.; Reade, A.; Mallory, M. J.; Glantz, S.; Weiner, O. D.; Lynch, K. W.; Gardner, K. H. An optogenetic gene expression system with rapid activation and deactivation kinetics. *Nat. Chem. Biol.* **2014**, *10*, 196−202.
(36) Cohen, R. N.; van der Aa, M. A. E. M.; Macaraeg, N.; Lee, A. P.; Szoka, F. C. Quantification of plasmid DNA copies in the nucleus after lipoplex and polyplex transfection. *J. Controlled Release* **2009**, *135*, 166−174.

(37) Malzahn, E.; Ciprianidis, S.; Káldi, K.; Schafmeier, T.; Brunner, M. Photoadaptation in Neurospora by Competitive Interaction of Activating and Inhibitory LOV Domains. *Cell* **2010**, *142*, 762−772.
(38) Heintzen, C.; Loros, J. J.; Dunlap, J. C. The PAS protein VIVID defines a clock-associated feedback loop that represses light input, modulates gating, and regulates clock resetting. *Cell* **2001**, *104*, 453−464.
(39) O'Neill, T. E.; Roberge, M.; Bradbury, E. M. Nucleosome arrays inhibit both initiation and elongation of transcripts by bacteriophage T7 RNA polymerase. *J. Mol. Biol.* **1992**, *223*, 67−78.
(40) Mazumder, B.; Seshadri, V.; Fox, P. L. Translational control by the 3′-UTR: The ends specify the means. *Trends Biochem. Sci.* **2003**, *28*, 91−98.
(41) Wang, X.; Le, N.; Denoth-Lippuner, A.; Barral, Y.; Kroschewski, R. Asymmetric partitioning of transfected DNA during mammalian cell division. *Proc. Natl. Acad. Sci. U. S. A.* **2016**, *113*, 7177−7182.
(42) Leppek, K.; Das, R.; Barna, M. Functional 5′ UTR mRNA structures in eukaryotic translation regulation and how to find them. *Nat. Rev. Mol. Cell Biol.* **2018**, *19*, 158−174.
(43) Martinez-Salas, E.; Francisco-Velilla, R.; Fernandez-Chamorro, J.; Embarek, A. M. Insights into structural and mechanistic features of viral IRES elements. *Front. Microbiol.* **2018**, *8*, 1−15.
(44) Gross, L.; Vicens, Q.; Einhorn, E.; Noireterre, A.; Schaeffer, L.; Kuhn, L.; Imler, J. L.; Eriani, G.; Meignin, C.; Martin, F. The IRES5′UTR of the dicistrovirus cricket paralysis virus is a type III IRES containing an essential pseudoknot structure. *Nucleic Acids Res.* **2017**, *45*, 8993−9004.
(45) Eisen, T. J.; Eichhorn, S. W.; Subtelny, A. O.; Lin, K. S.; McGeary, S. E.; Gupta, S.; Bartel, D. P. The Dynamics of Cytoplasmic mRNA Metabolism. *Mol. Cell* **2020**, *77*, 786−799.
(46) Wilusz, J. E.; JnBaptiste, C. K.; Lu, L. Y.; Kuhn, C. D.; Joshua-Tor, L.; Sharp, P. A. A triple helix stabilizes the 3′ ends of long noncoding RNAs that lack poly(A) tails. *Genes Dev.* **2012**, *26*, 2392−2407.
(47) Torabi, S. F.; Vaidya, A. T.; Tycowski, K. T.; DeGregorio, S. J.; Wang, J.; Shu, M. Di; Steitz, T. A.; Steitz, J. A. RNA stabilization by a poly(A) tail 3′-end binding pocket and other modes of poly(A)-RNA interaction. *Science* **2021**, DOI: 10.1126/science.abe6523.
(48) Russell, J. E.; Liebhaber, S. A. The stability of human β-globin mRNA is dependent on structural determinants positioned within its 3′ untranslated region. *Blood* **1996**, *87*, 5314−5323.
(49) Paddison, P. J.; Caudy, A. A.; Bernstein, E.; Hannon, G. J.; Conklin, D. S. Short hairpin RNAs (shRNAs) induce sequence-specific silencing in mammalian cells. *Genes Dev.* **2002**, *16*, 948−958.
(50) Wang, X.; Chen, X.; Yang, Y. Spatiotemporal control of gene expression by a light-switchable transgene system. *Nat. Methods* **2012**, *9*, 266−269.
(51) Triezenberg, S. J.; Kingsbury, R. C.; McKnight, S. L. Functional dissection of VP16, the trans-activator of herpes simplex virus immediate early gene expression. *Genes Dev.* **1988**, *2*, 718−729.
(52) Repina, N. A.; McClave, T.; Johnson, H. J.; Bao, X.; Kane, R. S.; Schaffer, D. V. Engineered Illumination Devices for Optogenetic Control of Cellular Signaling Dynamics. *Cell Rep.* **2020**, *31*, 107737.
(53) Yang, M. Y.; Chang, C. J.; Chen, L. Y. Blue light induced reactive oxygen species from flavin mononucleotide and flavin adenine dinucleotide on lethality of HeLa cells. *J. Photochem. Photobiol. B Biol.* **2017**, *173*, 325−332.
(54) Pryde, K. R.; Hirst, J. Superoxide is produced by the reduced flavin in mitochondrial complex I: A single, unified mechanism that applies during both forward and reverse electron transfer. *J. Biol. Chem.* **2011**, *286*, 18056−18065.
(55) Battich, N.; Stoeger, T.; Pelkmans, L. Control of Transcript Variability in Single Mammalian Cells. *Cell* **2015**, *163*, 1596−1610.
(56) Göpfrich, K.; Platzman, I.; Spatz, J. P. Mastering Complexity: Towards Bottom-up Construction of Multifunctional Eukaryotic Synthetic Cells. *Trends Biotechnol.* **2018**, *36*, 938−951.
(57) Buchan, J. R.; Parker, R. Eukaryotic Stress Granules: The Ins and Outs of Translation. *Mol. Cell* **2009**, *36*, 932−941.
(58) Van Treeck, B.; Protter, D. S. W.; Matheny, T.; Khong, A.; Link, C. D.; Parker, R. RNA self-assembly contributes to stress granule formation and defining the stress granule transcriptome. *Proc. Natl. Acad. Sci. U. S. A.* **2018**, *115*, 2734−2739.
(59) Wang, X.; Du, Q.; Zhang, W.; Xu, D.; Zhang, X.; Jia, Y.; Wang, T. Enhanced Transgene Expression by Optimization of Poly A in Transfected CHO Cells. *Front. Bioeng. Biotechnol.* **2022**, *10*, 722722.
(60) Shis, D. L.; Bennett, M. R. Synthetic biology: the many facets of T7 RNA polymerase. *Mol. Syst. Biol.* **2014**, *10*, 745.

https://doi.org/10.1021/acssynbio.2c00067
ACS Synth. Biol. 2022, 11, 2650−2661